Available online at www.sciencedirect.com
ScienceDirect
ELSEVIER
Progress in Natural Science: Materials International 20(2010) 61−69
Progress in Natural Science: Materials International
www.elsevier.com/locate/pnsc

Influence of Ru addition on microstructure and stress-rupture property of Ni-based single crystal superalloys

Jing-yang CHEN[1], Qiang FENG[1, 2], La-mei CAO[3], Zu-qing SUN[1]

1. State Key Laboratory for Advanced Metals and Materials, University of Science and Technology Beijing, Beijing 100083, China;
2. National Center for Materials Service Safety, University of Science and Technology Beijing, Beijing 100083, China;
3. National Key Laboratory of Science and Technology on Advanced High Temperature Structural Materials, Beijing Institute of Aeronautical Materials, Beijing 100095, China

Received 23 August 2010; accepted October 23 2010

Abstract: The effects of Ru on the microstructure and stress-rupture property were investigated in two experimental Ni-based single crystal superalloys with and without Ru addition (5.1%, mass fraction). The results indicate that the morphology of γ' precipitates in the dendrite core and interdendritic region are intermediate and nearly spherical, respectively, in the Ru-free alloy after being aged at 1 100 °C for 8 h. The Re partitioning ratio increases due to Ru addition and Ru partitioned preferentially to the γ phase in both dendrite core and interdendritic region of the Ru-containing alloy, which results in more negative lattice misfit and more cuboidal γ' precipitates. Meanwhile, the γ' volume fraction increases while the precipitate size and γ channel width decreases due to Ru addition in both dendrite core and interdendritic region. Ru addition improves the stress-rupture life at 1 100 °C/140 MPa significantly due to higher γ' volume fraction, more negative lattice misfit and a well rafting structure as well as less γ channel width.
Key words: Ni-based superalloys; ruthenium; elemental partitioning ratio; lattice misfit; γ' morphology; stress-rupture property

1 Introduction

Ni-based single crystal superalloys have been the primary materials for hot section components of advanced aero-engines due to their excellent high temperature properties. In the past decade, the research on the fourth generation single crystal superalloys, characterized by ruthenium (Ru) addition, has been more attractive in the international superalloy community. Ru addition has been reported to increase the liquidus temperatures[1], influence the microstructural stability[2−5] and creep property[6−10] of the Ni-based single crystal superalloys. However, the influence of Ru addition on the elemental partitioning behavior between γ and γ' phases, microstructural stability and high temperature creep property remains controversial. Understanding the relationship among Ru addition, γ/γ' elemental partitioning ratio and microstructural stability as well as high temperature creep resistance is essential for maximizing the potential benefits of this alloying element.

The influence of Ru addition on the partitioning behavior of alloying elements between γ and γ' phases is critical to the γ/γ' lattice misfit, γ' morphology and creep property. It is well accepted that the composition of γ and γ' phases controls the sign and magnitude of the lattice misfit, which influences the morphology of γ' precipitates[11] and the rafting behavior during creep deformation at high temperature[12]. It ultimately affects the creep property of single crystal superalloys. Early work suggested that Re did not partition strongly to the γ matrix due to Ru addition and suppressed the formation of topologically close-packed (TCP) phases[2]. However, there has been considerable disagreement on whether Ru causes "reverse partitioning" of alloying elements[4−5, 13]. Recently, high level of Ru addition was reported to increase the degree of Re and Cr supersaturation in the γ matrix and promoted the precipitation of TCP phases in a high Cr-containing Ni-based single crystal superalloy[5].

Foundation item: Project(2010CB631201) supported by the National Basic Research Program of China; Project(2007AA03A225) supported by the High Technology Research and Development Program of China; Project(50671015) supported by the National Natural Science Foundation of China; Project(NCET-06-0079) supported by the New Century Excellent Talents in University, Chinese Ministry of Education
Corresponding author: Qiang FENG; Tel: +86-10-62333584; E-mail: qfeng@skl.ustb.edu.cn

Regarding the effect of Ru addition on the creep property, YEH and his co-authors[7, 10] reported that Ru addition improved the creep resistance at high temperature and low stress by suppressing the formation of detrimental TCP phases effectively. However, YOKOKAWA et al[8] reported that the creep strength of TMS-82+ became worse due to Ru addition although TCP phase formation was completely suppressed. In addition, ZHANG et al[6] found that the interfacial dislocation spacing and the minimum creep rate increased under the effects of Ru addition in alloy TMS-75, and the creep resistance became worse. All these suggested that the mechanism by which Ru addition influence the creep property is still not well understood. Furthermore, there were limited systematic investigations regarding the influence of Ru addition on the morphology of γ' precipitates, γ/γ' elemental partitioning ratio and lattice misfit as well as phase stability, rafting behavior and creep resistance at high temperature and low stress.

In this study, the effect of Ru addition on the microstructure and stress-rupture property was investigated in two experimental Ni-based single crystal superalloys with and without Ru addition. Of particular interest was the influence of Ru addition on the γ' morphology, elemental partitioning behavior, lattice misfit, microstructural stability as well as stress-rupture property at high temperature and low stress (1 100 °C/ 140 MPa). Based on the microstructural investigations, the mechanisms by which Ru addition affects the microstructure and stress-rupture property were discussed.

2 Experimental

Two experimental alloys, designated USTB-F2 and USTB-F5, were directionally solidified as cylindrical single crystal bars with 14 mm in diameter and 150 mm in length. Their compositions were determined by an atomic absorption spectroscope as listed in Table 1. Alloy USTB-F2 is a Ru-free alloy and the baseline alloy in this study. Alloy USTB-F5 is similar to alloy USTB-F2 except for the addition of 5.1% Ru, which was substituted for Ni. It should point out that all the compositions were in the unite of mass fraction in this paper unless specially mentioned. The single crystal bars were solution treated at 1 330 °C for 6 h. The stress-rupture testing was conducted at 1 100 °C/140 MPa after the standard aging treatment (1 140 °C/8 h + 870 °C/16 h) and two specimens were tested for each investigated alloy. In order to investigate the effect of Ru addition on the tendency to form the rafting structure, the creep testing was performed at 1 100°C/130 MPa due to the limit of creep facilities and was interrupted at 1% creep strain.

Metallographic specimens were etched in a solution of 33% (volume fraction) acetic acid, 33% nitric acid, 33% deionized water and 1% hydrofluoric acid. And the microstructure was investigated using a ZEISS SUPRA 55 field-emission scanning electron microscope (FE-SEM) equipped with an energy-dispersive X-ray spectroscope (EDS). A back-scattered electron (BSE) detector was used to differentiate between the dendrite core and the interdendritic region. The volume fraction of γ' precipitates was determined using the standard point count method. And the γ' size and γ channel width were measured using the Image-Pro software. At least five images were used for determining the size and volume fraction of γ' precipitates as well as the width of γ channels in each alloy. The degree of the rafting behavior was characterized by the linear termination density, ρ_l, which represents physically the average number of terminations along a unit length of an individual γ' lamella[14]. The smaller the linear termination density, the more complete the rafting structure. Again, at least five images were used for determining the linear termination density in each alloy.

A JEOL JXA-8800R electron microprobe analyzer (EPMA) equipped with four wavelength-dispersive spectrometers (WDS) was used to determine the compositions of γ and γ' phases and investigate the partitioning behavior of alloying elements. Spot scans were conducted under an acceleration voltage of 20 kV, a beam current of 20 nA and a spot size of 1 μm. In order to minimize the matrix effect, some γ and γ' phases were apparently coarsened to at least 3 μm in size after thermal exposure at 1 100 °C for 800 h[15]. At least five WDS spectra were collected from γ and γ' phases for each experimental alloy. Partitioning ratio, k_i, was acquired through:

$$k_i = \frac{x_i^{\gamma}}{x_i^{\gamma'}} \tag{1}$$

where i represents each of the constituent elements, x_i^{γ}

Table 1 Measured compositions of two investigated alloys (mass fraction, %)

Alloy	Ni	Al	Ta	W	Co	Re	Cr	Ru
USTB-F2	Bal.	6.0	8.0	5.7	7.0	4.7	2.8	0
USTB-F5	Bal.	6.1	7.8	5.7	7.1	4.7	2.9	5.1

and $x_i^{\gamma'}$ correspond to the mole concentration of element i in γ and γ' phases, respectively. The lattice parameters of the γ and γ' phases were calculated by the formula presented by Ref.[16] according to EPMA results. Subsequently, the γ/γ' lattice misfit (δ) is calculated by the following equation:

$$\delta = \frac{2(a_{\gamma'} - a_{\gamma})}{a_{\gamma'} + a_{\gamma}} \quad (2)$$

where a_{γ} and $a_{\gamma'}$ are the lattice parameters of γ and γ' phases, respectively.

3 Results

3.1 Characteristics of γ' precipitates

The typical microstructures of the two investigated alloys after being aged at 1 100 °C for 8 h are shown in Fig.1. The morphology, volume fraction and size of γ' precipitates as well as the width of γ channels for two investigated alloys are listed in Table 2. The γ' morphology was defined in detail in Ref.[15]. The morphology of γ' precipitates was intermediate and nearly spherical in the dendrite core and interdendritic region of alloy USTB-F2 (Ru-Free), respectively (Figs.1(a1) and (a2)). After the addition of Ru, it became cuboidal and nearly cuboidal in the dendrite core and interdendritic region of alloy USTB-F5, respectively (Figs.1(b1) and (b2)). Meanwhile, the volume fraction of γ' precipitates increased while the precipitate size and γ channel width decreased under the influence of Ru in both dendrite core and interdendritic region. The γ' volume fractions in the dendrite core and interdendritic region of alloy USTB-F2 were 55.1% and 63.5%, respectively, and they increased to 61.0% and 67.0% in alloy USTB-F5. In addition, the width of γ channel in the dendrite core and interdendritic region of Ru-containing alloy USTB-F5 was 45 nm and 62 nm, respectively, which was about 58% and 65% of that of alloy USTB-F2 (Ru-free).

3.2 Long-term microstructural stability

Figure 2 shows the typical microstructures in the dendrite core of two investigated alloys after being aged at 1 100 °C for 2 000 h. The γ' precipitates only coarsened and some of them began to coalesce, but did not raft even after thermal exposure for 2 000 h in the Ru-free alloy USTB-F2. Meanwhile, no secondary precipitates were found to exist (Fig.2(a)). However, alloy USTB-F5 rafted significantly. And very limited secondary precipitates, marked by arrows, were observed in the dendrite core of alloy USTB-F5 (Fig.2(b)). The EDS results indicated that these precipitates were enriched in Re and Ru. It should be the hexagonal δ phase according to its composition feature[17]. In addition, it should be noted that no secondary phase was observed in the interdendritic region of both alloys

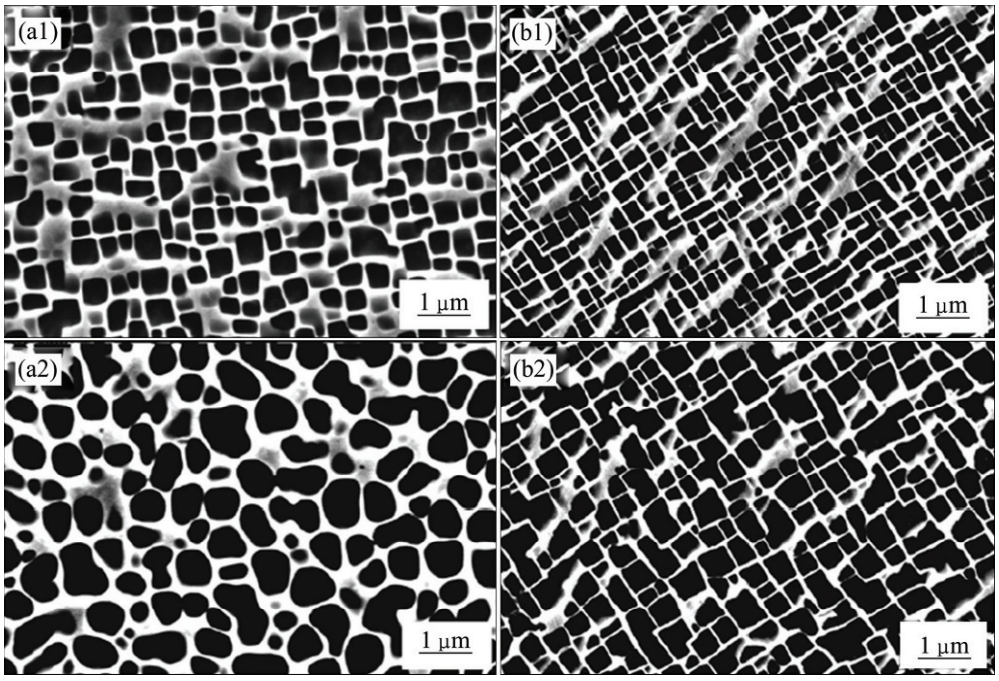

Fig.1 Typical microstructures of alloys USTB-F2(a) and USTB-F5(b) after being aged at 1 100 °C for 8 h: (a1, b1) Taken in dendrite core; (a2, b2) Taken in interdendritic region

Table 2 Morphology, volume fraction and size of γ' precipitates as well as width of γ channels in two investigated alloys after being aged at 1 100 °C for 8 h

Alloy	Dendrite core				Interdendritic region			
	γ' precipitate morphology	γ' volume fraction /%	γ' size/μm	γ channel width /nm	γ' precipitate morphology	γ' volume fraction/%	γ' size/μm	γ channel width/nm
USTB-F2	Intermediate	55.1±0.8	0.37±0.12	77±22	Nearly spherical	63.5±1.0	0.55±0.10	95±38
USTB-F5	Cuboidal	61.0±0.7	0.28±0.09	45±13	Nearly cuboidal	67.0±1.1	0.47±0.10	62±22

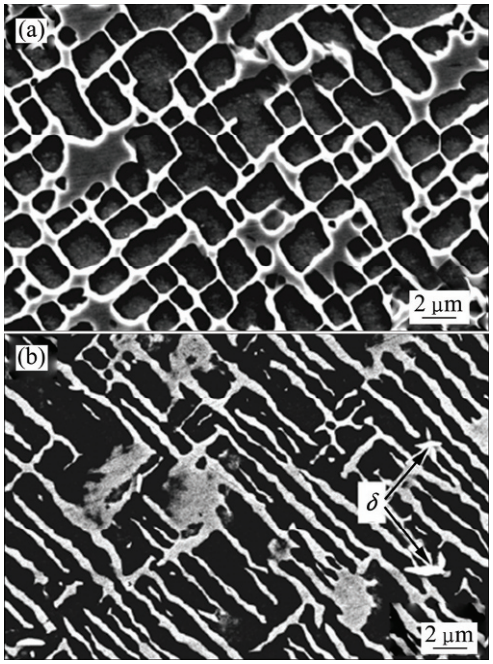

Fig.2 Typical microstructures in dendrite core of alloys USTB-F2(a) and USTB-F5(b) after thermal exposure at 1 100 °C for 2 000 h

3.3 Elemental partitioning ratio and lattice misfit

The compositions of γ and γ' phases and the associated elemental partitioning ratios are listed in Tables 3 and 4, respectively. Although slight differences of partitioning behaviors for other alloying elements may have been present, the partitioning behaviors of Re and Cr changed most evidently due to Ru addition in the dendrite core of two investigated alloys. Re and Cr partitioned preferentially to the γ phase, and the partitioning ratios of Re and Cr increased from 5.50 and 1.75 in alloy USTB-F2 (Ru-free) to 6.71 and 2.21 in alloy USTB-F5 (5.1% Ru), respectively.

In the interdendritic region, the Re concentration of the γ phase in alloy USTB-F2 was 2.2% (mole fraction). More Re partitioned to the γ phase and the Re content in the γ phase of Ru-containing alloy USTB-F5 was 3.3% (mole fraction). Meanwhile, the Re concentration in γ' precipitates decreased slightly. So the Re partitioning ratio increased from 3.14 to 6.60 (Table 4). The partitioning behaviors of other alloying elements changed slightly, but with less pronounced characteristics than Re. In addition, Ru partitioned to the γ matrix mildly in both dendrite core and interdendritic region of alloy USTB-F5.

The lattice misfits are also listed in Table 3, and they were calculated based on the compositions of γ and γ' phases and the formula in Ref.[16]. The lattice misfits in the dendrite core and interdendritic region of the baseline alloy USTB-F2 were −0.22% and −0.01%, respectively. They became more negative in both dendrite core and interdendritic region in alloy USTB-F5 containing Ru, and they were −0.54% and −0.35%, respectively.

3.4 Stress-rupture properties and post-creep microstructures

The stress-rupture properties of the two investigated alloys at 1 100 °C/140 MPa are listed in Table 5. The average stress-rupture life of Ru-free alloy USTB-F2 was 73.0 h. And the average stress-rupture life of Ru-containing alloy USTB-F5 was 176.4 h, which was 2.4 times that of alloy USTB-F2. In addition, both alloys possessed good high-temperature ductility.

Alloys USTB-F2 and USTB-F5 crept to 1% strain at 1 100 °C/130 MPa for 39 h and 106 h, respectively. Subsequently, post-creep microstructures were examined on (010), (100) and (001) sections. The three-dimensional post-creep microstructures of two investigated alloys after 1% creep deformation are shown in Fig.3. The linear termination densities of two investigated alloys are listed in Table 6. In the dendrite core (Figs.3(a1) and (b1)), both Ru-free alloy and Ru-containing alloy rafted perpendicular to the stress axis on the surfaces of (100) and (010) after creep deformation. It should be noted that the linear termination density decreased from alloy USTB-F2 to alloy USTB-F5 (Table 6), and it is suggested that the degree of rafting behavior increased under the influence of Ru addition. In the interdendritic region, no rafting occurred in alloy USTB-F2 (Fig.3(a2)) and the linear termination density could not be determined. However, alloy USTB-F5 rafted perpendicularly to the stress axis in the longitudinal-section, as shown in Fig.3(b2). In

Table 3 Compositions of elements in γ and γ' phases (mole fraction, %) and calculated lattice misfit (δ) for two investigated alloys after thermal exposure at 1 100 °C for 800 h

Alloy	Region	Phase	Mole fraction/%							Lattice misfit, δ/%
			Al	Ta	W	Co	Re	Cr	Ru	
USTB-F2	Dendrite core	γ	8.2	1.6	2.3	9.2	4.4	4.9	−	−0.22
		γ'	15.2	3.4	1.7	6.2	0.8	2.8	−	
	Interdendritic region	γ	8.9	2.3	2.0	7.9	2.2	4.4	−	−0.01
		γ'	16.8	3.5	1.6	4.8	0.7	1.9	−	
USTB-F5	Dendrite core	γ	8.4	1.3	2.4	9.4	4.7	5.3	4.7	−0.54
		γ'	15.4	3.5	1.8	5.8	0.7	2.4	2.8	
	Interdendritic region	γ	8.8	2.2	2.1	8.1	3.3	4.5	4.0	−0.35
		γ'	16.4	3.7	1.7	5.0	0.5	1.8	2.6	

Table 4 Elemental partitioning ratios (k_i) of γ and γ' phases for two investigated alloys after thermal exposure at 1 100 °C for 800 h

Alloy	Region	k_i						
		Al	Ta	W	Co	Re	Cr	Ru
USTB-F2	Dendrite core	0.54	0.47	1.35	1.48	5.50	1.75	−
	Interdendritic region	0.53	0.66	1.25	1.65	3.14	2.32	−
USTB-F5	Dendrite core	0.55	0.37	1.33	1.62	6.71	2.21	1.68
	Interdendritic region	0.54	0.59	1.24	1.62	6.60	2.50	1.54

Table 5 Stress-rupture properties of two investigated alloys at 1 100 °C/140 MPa

Alloy	Specimen No.	Stress-rupture life/h	Average stress-rupture life/h	Elongation/%	Area reduction/%
USTB-F2	2-1	69.2	73.0±5.4	42.8	57.5
	2-2	76.8		49.6	51.8
USTB-F5	5-1	176.3	176.4±0.1	57.2	46.7
	5-2	176.4		57.2	38.2

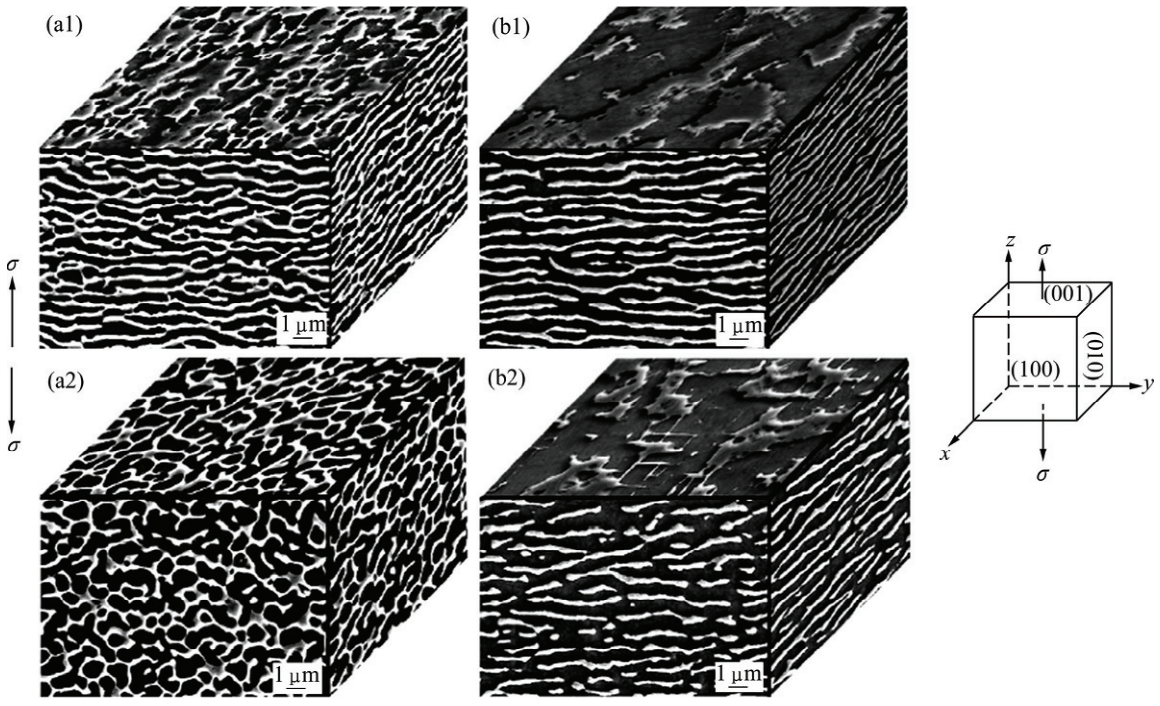

Fig.3 Post-crept microstructures of alloys USTB-F2(a) and USTB-F5(b) after creep testing at strain of 1% under 1 100 °C/130 MPa (Applied tensile stress is in vertical direction and in plane of page): (a1, b1) Taken in dendrite core; (a2, b2) Taken in interdendritic region

addition, no secondary phase precipitated in both dendrite core and interdendritic region of alloys USTB-F2 and USTB-F5 after stress-rupture and creep deformation.

Table 6 Linear termination densities after 1% creep stain and time to 1% creep strain at 1 100 °C/130 MPa

Alloy	Linear termination density/10^2 mm^{-1}		Time to 1% creep strain/h
	Dendrite core	Interdendritic region	
USTB-F2	3.13±0.33	−	39
USTB-F5	1.52±0.23	1.89±0.21	106

Note: Symbol "−" represents that alloy does not raft after 1% creep strain and linear termination density could not be determined.

4 Discussion

It is known that γ/γ' lattice misfit influences the morphology of γ' precipitates[11, 18−20], mechanical properties[6, 21] and phase stability [15, 22] of Ni-based single crystal superalloys. FÄHRMANN et al[11] investigated the influence of the sign and magnitude of the lattice misfit on the morphology of γ' precipitates in Ni-Al-Mo ternary alloys. γ' precipitates were spherical in alloys with a near zero misfit, whereas they became cuboidal when the lattice misfit deviated from zero in either the positive or negative direction. Recently, the phase-field simulation results show good agreement with the above mentioned experimental results[18]. In addition, the lattice misfit is the driving force for the rafting behavior during creep deformation and is known to enhance the creep property at high temperature and low stress[6]. Ni-based single crystal superalloys that raft perpendicular to the applied tensile stress have a negative lattice misfit. And alloys with a positive lattice misfit raft parallel to the applied tensile stress. If the lattice misfit is eliminated, the rafting structure should not occur[12]. Meanwhile, the coherency stress between γ and γ' phases induced by the lattice misfit was reported to increase the kinetics of γ' coarsening and rafting during un-stressed long-term thermal exposures[15, 22].

4.1 Elemental partitioning ratio, lattice misfit, γ' morphology and microstructural stability

Thermodynamically, the TCP precipitation is controlled by the degree of supersaturation of TCP-forming elements in the γ matrix, most notably by refractory elements such as Re, W and Mo. Early work suggested that Ru addition decreased the degree of Re supersaturation in the γ phase and suppressed the formation of TCP phases. This behavior is so-called "reverse partitioning effect" of Ru[2]. Since then, there has been considerable disagreement on whether Ru causes "reverse partitioning" of alloying elements, since Ru did not induce remarkable changes of elemental partitioning behavior in other studies. Re partitioning ratio was reported to be most strongly influenced by the Co content, while increasing the Co addition reduced the Re partitioning ratio[23]. The Co content of the current experimental alloys (7.0%) was significantly lower than that of the alloys reported in Ref.[2], which contained very high level of Co (up to 20%). Likewise, OFORI et al[24]. investigated platinum group metal additions to an experimental Ni-based superalloy and reported that increasing Ru content resulted in less Re partitioning to the γ matrix in a Cr-free alloy. Recently, CARROLL et al[19] reported that Re partitioning ratios were similar in Cr-free alloys containing various levels of Ru additions, which ranged from 5.7% to 9.6%. All these suggest that elemental partitioning behaviors are very complex in multi-component Ni-based superalloys over a broad range of compositions.

In this study, both alloys contained a medium level of Cr (2.8%). The major composition difference between two alloys was the Ru content (5.1%). Re partitioned preferentially to the γ phase due to Ru addition in both dendrite core and interdendritic region. In addition, Ru partitioned to the γ matrix in both dendrite core and interdendritic region of alloy USTB-F5 (Table 4). According to the Eq.(2), the strong Re partitioning to the γ matrix caused by Ru addition and the partitioning behavior of Ru result in more negative lattice misfit since both Re and Ru have larger atomic radii in comparison to Ni. Meanwhile, γ' precipitates became more cuboidal under the influence of Ru addition in both dendrite core and interdendritic region (Fig.1). The changes of γ' morphology and Re partitioning ratio as well as the partitioning behavior of Ru show good agreement with the change of the lattice misfit (Table 3). Besides the change in γ' morphology, more negative lattice misfit induced by Ru addition also accelerated the coarsening and rafting of γ' precipitates during un-stressed thermal exposure at 1 100 °C (Fig.2). In addition, high level of Ru addition induced the precipitation of δ phase enriched in Re and Ru in the dendrite core of the Ru-containing alloy during long-term thermal exposure (Fig.2(b)).

4.2 Stress-rupture properties

Ru addition was reported to influence the creep property of Ni-based single crystal superalloys[6−10, 25]. ZHANG et al[6] found that the γ/γ' interfacial dislocation networks played an important role during creep. The

finer the interfacial dislocation networks, the smaller the minimum creep rate and the longer the creep life. YEH et al[7, 10] reported that Ru effectively hindered the precipitation of TCP phases and maintained the continuity of the rafting microstructure; it became the primary factor to improve the creep resistance at high temperature and low stress. Although changes in lattice misfits and dislocation networks due to Ru addition were also observed, their effects on the creep life appeared to be minimal. YOKOKAWA et al[8] reported that the creep strength of TMS-82+ at 1 100 °C/137 MPa became worse after the addition of 2.0% Ru although TCP phase formation was completely suppressed because Ru is not an effective element for solid solution strengthening at high temperature. To date, the mechanisms by which Ru influences the creep property remain debatable. In this study, the present results indicated that high temperature creep and stress-rupture property of Ni-based single crystal superalloys were influenced by Ru addition in these following factors, such as volume fraction of γ' precipitates, γ/γ' lattice misfit, rafting behavior during creep, γ channel width, degree of solid solution strengthening and microstructural stability.

4.2.1 Effect of γ' volume fraction and γ channel width

Ni-based single crystal superalloys usually consist of high volume fraction of ordered γ' precipitates (with a $L1_2$ structure) in coherent with the disordered FCC γ matrix. Previous investigation indicated that the optimized volume fraction of γ' precipitates to result in the peak creep strength was at around 65%−70%[26]. In the current study, the γ' volume fraction of alloy USTB-F5 was higher than that of alloy USTB-F2 (Table 2). So, the structural hardening induced by γ' precipitates was higher in alloy USTB-F5 than that in alloy USTB-F2. Early work suggested that Ru addition destabilizes the γ' precipitates at elevated temperatures[4, 27], which is clearly different with the current work. This might be due to the complex influence of Ru addition on the stability of γ' precipitates in multicomponent Ni-based single crystal superalloys over a broad range of compositions. In addition, it should be noted that the Al content in alloy USTB-F5 was 0.5% (mole fraction) higher than that of alloy USTB-F2, and it also resulted in higher volume fraction of γ' precipitates in alloy USTB-F5.

Pollock and Argon [21] reported that the Orowan resistance (τ_{OR}) to the bowing of dislocations through narrow matrix channels can be calculated as:

$$\tau_{OR} = \sqrt{\frac{2}{3}}\frac{\mu b}{l} \tag{3}$$

where μ is the shear modulus, b is the Burgers vector and l is the γ channel width. In this study, the γ channels in both dendrite core and interdendritic region of alloy USTB-F5 were narrower than that of alloy USTB-F2 (Fig.1 and Table 2). Assuming μ=48.2 GPa and b=0.254 nm[20−21], the uniaxial applied stresses required for bowing dislocations through the matrix channel are 318 MPa and 258 MPa in the dendrite core and interdendritic region of alloys USTB-F2, respectively, taking into account a [001] Schmid factor of 0.408. And they were 544 MPa and 395 MPa in the dendrite core and interdendritic region of alloys USTB-F5, respectively. Therefore, the Orowan resistance of alloy USTB-F5 was higher than that of alloy USTB-F2.

4.2.2 Effect of lattice misfit, γ' morphology and rafting behavior

In the current study, both Ru-free alloy and Ru-containing alloy rafted perpendicular to the stress axis in the dendrite core (Figs.3(a1) and (b1)). However, it is worthy of noting that alloy USTB-F5 with cuboidal γ' precipitates rafted more completely than alloy USTB-F2 containing intermediate γ' precipitates since the linear termination density of alloy USTB-F5 was less than the half of alloy USTB-F2 (Table 6). The change of the above two factors (γ' morphology and rafting behavior) shows good agreement with the change of lattice misfit (Table 3). In the interdendritic region, alloy USTB-F2 with nearly spherical γ' precipitates and close to zero lattice misfit did not raft (Fig.3(a2)). However, alloy USTB-F5 with nearly cuboidal γ' precipitates (Fig.1(b2)) and negative lattice misfit rafted perpendicularly to the stress axis (Fig.3(b2)). The rafting behavior was also consistent with the γ' morphology and lattice misfit. The creep property of single crystal superalloys usually increased with the increasingly negative lattice misfit because the net stress in γ channels decreased when the lattice misfit became more negative for loading along the 〈001〉 direction[28]. In addition, the precipitate shearing and the creation of an anti-phase boundary (APB) in ordered γ' precipitates are not necessary for the continued deformation if the matrix channels parallel to the stress axis have not been eliminated [20]. There also left many γ channels parallel to the stress axis in alloy USTB-F2 after 1% creep strain (Figs.3(a1) and (a2)). However, γ channels parallel to the stress axis were almost eliminated in both dendrite core and interdendritic region of alloy USTB-F5 (Figs.3(b1) and (b2)). Accordingly, the average stress-rupture life of Ru-containing alloy was longer than that of the Ru-free alloy. Similar features have been reported in UM-F series alloys[20, 29] and in other USTB-F series alloys[25].

4.2.3 Effect of solid solution strengthening and microstructural stability

As the most effective solid solution strengthening

element, Re is known to play a significant role in improving the creep property of superalloys because of its tendency to form clusters[30] and low diffusivity[31]. In this study, the Re concentrations of the γ phase were very close in the dendrite cores of alloys USTB-F2 and USTB-F5. However, Re partitioned preferentially to the γ matrix in the interdendritic region due to Ru addition and the Re concentration in the γ matrix of alloy USTB-F5 was 50% higher than that of alloy USTB-F2 (Table 3). Therefore the solid solution strengthening of Re in the interdendritic region of alloy USTB-F5 was higher than that of alloy USTB-F2. Creep cavitations usually initiated in the residual eutectic and casting porosities in the interdendritic region as well as brittle phases such as TCP phases due to the stress concentration[32−34]. It should be noted that the residual eutectic in both experimental alloys was in the same level. Meanwhile, as mentioned previously, there was no secondary phase in both dendrite core and interdendritic region of two investigated alloys after stress-rupture and creep deformation (Fig.3). The higher contribution of Re to the solid solution strengthening may retard the initiation of creep cavitation in the interdendritic region of alloy USTB-F5. In addition, the current study indicates that Ru partitioned preferentially to the γ phase in both dendrite core and interdendritic region of alloy USTB-F5 (Table 4). However, early work suggested that Ru was not an effective solid solution strengthener at high temperature[7− 8, 10].

The results of microstructural stability during un-stressed thermal exposure at 1 100 °C confirmed that the addition of Ru promoted the precipitation of δ phase. However, no δ phase formed in alloys USTB-F2 and USTB-F5 after stress-rupture and creep deformation because both stress-rupture life and creep time are insufficient to initiate the precipitation of δ phase.

5 Conclusions

1) The γ' precipitates in the dendrite core and interdendritic region of the Ru-free alloy after being aged at 1 100 °C for 8 h were intermediate and nearly spherical, respectively. Re and Ru partitioned preferentially to the γ phase in both dendrite core and interdendritic region of the Ru-containing alloy, resulting in more negative lattice misfit and more cuboidal γ' precipitates.

2) Ru addition increased the stress-rupture life at 1 100 °C/140 MPa significantly since it increased the γ' volume fraction and decreased the γ channel width as well as more negative lattice misfit with a well rafting structure perpendicular to the applied tensile stress in both dendrite core and interdendritic region.

Acknowledgments

The authors would like to acknowledge useful discussions with Y.R. ZHENG. The authors are also grateful to J.P. HE, B. ZHAO and P.P. HU for their assistance with SEM analyses and sample preparation.

References

[1] FENG Q, NANDY T K, TIN S, POLLOCK T M. Solidification of high-refractory ruthenium-containing superalloys[J]. Acta Materialia, 2003, 51(1): 269−284.

[2] O'HARA K S, WALSTON W S, ROSS E W, DAROLIA R. Nickle base superalloy and article. US Patent 5,482,789[P]. 1996.

[3] SATO A, HARADA H, YOKOKAWA T, MURAKUMO T, KOIZUMI Y, KOBAYASHI T, IMAI H. The effects of ruthenium on the phase stability of fourth generation Ni-base single crystal superalloys[J]. Scripta Materialia, 2006, 54(9): 1679−1684.

[4] HOBBS R A, ZHANG L, RAE C M F, TIN S. Mechanisms of topologically close-packed phase suppression in an experimental ruthenium-bearing single-crystal nickel-base superalloy at 1 100 ℃ [J]. Metallurgical and Materials Transactions A, 2008, 39(5): 1014−1025.

[5] CHEN J Y, FENG Q, SUN Z Q. Topologically close-packed phase promotion in a Ru-containing single crystal superalloy[J]. Scripta Materialia, 2010, 63(8): 795−798.

[6] ZHANG J X, MURAKUMO T, HARADA H, KOIZUMI Y. Dependence of creep strength on the interfacial dislocations in a fourth generation SC superalloy TMS-138[J]. Scripta Materialia, 2003, 48(3): 287−293.

[7] YEH A C, RAE C M F, TIN S. High temperature creep of Ru-bearing Ni-base single crystal superalloys[C]// GREEN K A, POLLOCK T M, HARADA H, HOWSON T E, REED R C, SCHIRRA J J, WALSTON S. Superalloys 2004. Champion, PA: TMS, 2004: 677−685.

[8] YOKOKAWA T, KOIZUMI Y, KOBAYASHI T, HARADA H. Effect of Re and Ru additions to second generation nickel-base single crystal superalloy TMS-82+[J]. Journal of the Japan Institute of Metals, 2006, 70(8): 670−673.

[9] ZHENG L, LI S, XIAO C, TANG D, GU C. Microstructure and high temperature stress rupture properties of Ru-containing directionally solidified Ni-base superalloy[J]. Key Engineering Materials, 2007, 353−358: 507−510.

[10] TIN S, ZHANG L, HOBBS R, YEH A C, RAE C, BROOMFIELD B. Linking the properties, processing and chemistry of advanced single crystal Ni-base superalloys[C]// REED R C, GREEN K A, CARON P, GABB T P, FAHRMANN M G, HURON E S, WOODARD S A. Superalloys 2008. Champion, PA: TMS, 2008: 81−90.

[11] FÄHRMANN M, FRATZL P, PARIS O, FÄHRMANN E, JOHNSON W C. Influence of coherency stress on microstructural evolution in model Ni-Al-Mo alloys[J]. Acta Metallurgica et Materialia, 1995, 43(3): 1007−1022.

[12] FÄHRMANN M, HERMANN W, FÄHRMANN E, BOEGLI A, POLLOCK T M, SOCKEL H G. Determination of matrix and precipitate elastic constants in (γ-γ') Ni-base model alloys, and their relevance to rafting[J]. Materials Science and Engineering A, 1999, 260(1/2): 212−221.

[13] VOLEK A, PYCZAK F, SINGER R F, MUGHRABI H. Partitioning of Re between γ and γ' phase in nickel-base superalloys[J]. Scripta Materialia, 2005, 52(2): 141−145.

[14] NATHAL M. Effect of initial gamma prime size on the elevated temperature creep properties of single crystal nickel base superalloys[J]. Metallurgical and Materials Transactions A, 1987,

18(11): 1961−1970.

[15] CHEN J Y, ZHAO B, FENG Q, CAO L M, SUN Z Q. Effects of Ru and Cr on γ/γ' microstructural evolution of Ni-based single crystal superalloys during heat treatment[J]. Acta Metallurgica Sinica, 2010, 46(8): 897−906. (in Chinese)

[16] KABLOV E N, PETRUSHIN N V. Designing of high-rhenium single crystal Ni-base superalloy for gas turbine blades[C]// REED R C, GREEN K A, CARON P, GABB T P, FAHRMANN M G, HURON E S, WOODARD S A. Superalloys 2008. Champion, PA: TMS, 2008: 901−908.

[17] FENG Q, NANDY T K, POLLOCK T M. The Re (Ru)-rich δ-phase in Ru-containing superalloys[J]. Materials Science and Engineering A, 2004, 373(1/2): 239−249.

[18] WANG T, SHENG G, LIU Z K, CHEN L Q. Coarsening kinetics of γ' precipitates in the Ni-Al-Mo system[J]. Acta Materialia, 2008, 56(19): 5544−5551.

[19] CARROLL L J, FENG Q, MANSFIELD J F, POLLOCK T M. Elemental partitioning in Ru-containing nickel-base single crystal superalloys[J]. Materials Science and Engineering A, 2007, 457(1/2): 292−299.

[20] CARROLL L J, FENG Q, MANSFIELD J F, POLLOCK T M. High refractory, low misfit Ru-containing single-crystal superalloys[J]. Metallurgical and Materials Transactions A, 2006, 37(10): 2927−2938.

[21] POLLOCK T M, ARGON A S. Creep resistance of CMSX-3 nickel base superalloy single crystals[J]. Acta Metallurgica et Materialia, 1992, 40(1): 1−30.

[22] PYCZAK F, DEVRIENT B, NEUNER F C, MUGHRABI H. The influence of different alloying elements on the development of the γ/γ' microstructure of nickel-base superalloys during high-temperature annealing and deformation[J]. Acta Materialia, 2005, 53(14): 3879−3891.

[23] WALSTON S, CETEL A, MACKAY R, O'HARA K, DUHL D, DRESHFIELD R. Joint development of a fourth generation single crystal superalloy[C]// GREEN K A, POLLOCK T M, HARADA H, HOWSON T E, REED R C, SCHIRRA J J, WALSTON S. Superalloys 2004. Champion, PA: TMS, 2004: 15−24.

[24] OFORI A P, HUMPHREYS C J, TIN S, JONES C N. A TEM study of the effect of platinum group metals in advanced single crystal nickel-base superalloys[C]// GREEN K A, POLLOCK T M, HARADA H, HOWSON T E, REED R C, SCHIRRA J J, WALSTON S. Superalloys 2004. Champion, PA: TMS, 2004: 787−793.

[25] CHEN J Y, HU P P, FENG Q, CAO L M, SUN Z Q. Ru effects on microstructural evolution during thermal exposure and stress-rupture property of Ni-based single crystal superalloys[J]. Rare Metal Materials and Engineering, in press. (in Chinese)

[26] MURAKUMO T, KOBAYASHI T, KOIZUMI Y, HARADA H. Creep behaviour of Ni-base single-crystal superalloys with various γ' volume fraction[J]. Acta Materialia, 2004, 52(12): 3737−3744.

[27] YEH A C, TIN S. Effects of Ru on the high-temperature phase stability of Ni-base single-crystal superalloys[J]. Metallurgical and Materials Transactions A, 2006, 37(9): 2621−2631.

[28] HARADA H, MURAKAMI H. Design of Ni-base superalloys[M]. Heidelberg, Berlin: Springer-Verlag, 1999: 53−55.

[29] CARROLL L J, FENG Q, POLLOCK T M. Interfacial dislocation networks and creep in directional coarsened Ru-containing nickel-base single-crystal superalloys[J]. Metallurgical and Materials Transactions A, 2008, 39(6): 1290−1307.

[30] BLAVETTE D, CARON P, KHAN T. An atom probe investigation of the role of rhenium additions in improving creep resistance of Ni-base superalloys[J]. Scripta Metallurgica, 1986, 20(10): 1395−1400.

[31] GIAMEI A, ANTON D. Rhenium additions to a Ni-base superalloy: Effects on microstructure[J]. Metallurgical and Materials Transactions A, 1985, 16(11): 1997−2005.

[32] REED R C, MATAN N, COX D C, RIST M A, RAE C M F. Creep of CMSX-4 superalloy single crystals: Effects of rafting at high temperature[J]. Acta Materialia, 1999, 47(12): 3367−3381.

[33] LIU L R, JIN T, ZHAO N R, WANG Z H, SUN X F, GUAN H R, HU Z Q. Stress rupture properties and fracture behavior of a Ni base single crystal superalloy allong [001] direction[J]. Acta Metallurgica Sinica, 2004, 40(8): 858−862. (in Chinese)

[34] MA W Y, LI S S, QIAO M, GONG S K, ZHENG Y R, HAN Y F. Effect of heat treatment on microstructure and stress rupture life of Ni-base single crystal superalloy[J]. The Chinese Journal of Nonferrous Metals, 2006, 16(6): 937−944. (in Chinese)